Research Paper

Full visible-light absorption of TiO_2 nanotubes induced by anionic S_2^{2-} doping and their greatly enhanced photocatalytic hydrogen production abilities

Shuchao Sun [a,1], Jianjiao Zhang [a,1], Peng Gao [a,*], Ying Wang [a], Xiaobo Li [a], Tingting Wu [a], Yanbo Wang [a], Yujin Chen [b,*], Piaoping Yang [a,*]

[a] Key Laboratory of Superlight Materials and Surface Technology, Ministry of Education, College of Materials Science and Chemical Engineering, Harbin Engineering University, Nantong Street 145, Harbin, Heilongjiang, 150001, PR China
[b] College of Science, Harbin Engineering University, Nantong Street 145, Harbin, Heilongjiang, 150001, PR China

ARTICLE INFO

ABSTRACT

TiO_2, as a benchmark photocatalyst for hydrogen production through water splitting, has a relatively large band gap (3.2 eV for anatase and 3.0 eV for rutile) requiring UV light (290–400 nm) for electronic excitations from the valence band to the conduction band, hence utilizing only a small part of the solar spectrum. The construction of new electronic band gap, especially in the visible region (400–800 nm), is of great importance for improving TiO_2 optical and photocatalytic properties. In this work, though it is deem metastable and can induce a broad visible-light adsorption in previous literatures, anionic S_2^{2-} has been successfully introduced into TiO_2 nanotubes, which is different from the previous works about S-doped TiO_2 that contain only cationic S^{4+} and S^{6+}. Resultantly, the S_2^{2-} doped TiO_2 nanotubes exhibit a full visible-light absorption (from 400 to 800 nm) and a greatly enhanced photocatalytic H_2-production rate under visible-light irradiation (9610 μmol h^{-1} g^{-1}, about 13.7 and 37 times of other cationic and anion S-doped TiO_2 nanoparticles, respectively, almost highest in all the results reported previously in literatures of TiO_2 doped with non-metal elements).

© 2017 Elsevier B.V. All rights reserved.

1. Introduction

The increasingly serious energy crisis and the environmental contamination caused by the burning of fossil fuels have led to an aggressive search for renewable and environmental-friendly alternative energy recourses [1]. Hydrogen energy has been recognized as a potentially significant alternative form of storable and clean energy for the future. Since the discovery of water photolysis on a TiO_2 photoanode in the 1970s [2], it has attracted significant attention due to its promising applications in environment remediation and solar energy conversion in the past decades [3–7]. As an initial semiconductor photocatalyst investigated, TiO_2 is still regarded as a benchmark photocatalyst under ultraviolet irradiation due to its intrinsic high activity. However, TiO_2 is a type of wide bandgap semiconductor (3.2 eV for anatase and 3.0 eV for rutile) and mainly adsorbs ultraviolet light (290–400 nm), which greatly limits its practical applications in the visible light [8]. Accordingly, persistent efforts have been made to narrow the bandgap of TiO_2 to extend its working spectrum to the visible light region.

Recent researches on TiO_2 doping with nonmetal elements (such as S), have proved the validity of this method in narrowing the TiO_2 band gap, though the band-gap isn't modified enough for visible-light absorption [9–19]. At the same time, the origin of the visible-light responsive S-doped TiO_2 remains unclear and its full visible-light absorption is still on the way, which is determined by the chemical nature (anionic S^{2-} or cationic S^{4+} and S^{6+}) and the structural location (substitutional, interstitial, etc.) of the S-doping species. However, in previous experimental works about S-doped TiO_2, only cationic S^{4+} and S^{6+} in the substitution of Ti^{4+} have been obtained [15,20–22], which only displayed slight optical absorption shift from UV region to visible-light region (near 400 nm). Interestingly, it was found that S^{2-} species showed a visible light absorption through an oxidization of TiS_2 [15]. In addition, it was also predicted though a theory calculation that anionic S (isolates S^{2-}, S_2^{2-}) showed completely different spectral behaviors compared with that of undoped TiO_2 and TiO_2 doped of cationic S^{4+} and S^{6+},

which had rarely been observed in the experimental optical spectra for S-doped TiO_2 [27]. More importantly, anionic S_2^{2-} doped TiO_2 possessed a very wide visible-light absorption region ranged from 400 to 700 nm because new occupied and strongly localized electronic states in the gap, located at 0.9–1.6 eV above the valence band of TiO_2, have been formed [24]. Otherwise, another advantage of S_2^{2-} over the cationic S^{4+} and S^{6+} should be highlighted. In general there are a large number of O vacancies on the TiO_2 surface, which act as the electron-hole recombination centers and reduce photocatalytic H_2-production rate. So S_2^{2-} doped TiO_2 material should have a greatly enhanced photocatalytic H_2-production rate under visible-light irradiation.

However, it has been proved that cationic S-doping of TiO_2 (S^{4+} or S^{6+}) is much more stable than anionic doping and its exothermicity is also significantly higher than for anionic doping, and consequently the cationic doping appears as the most probable state, while anionic doping is metastable. In order to realize the anionic doping, in this work layer-structured TiO_2 nanotubes with tiny size were selected by us as the precursor, whose special structure made it possess a high reaction activity and facilitate the diffusion of S_2^{2-} into TiO_2. And S_2^{2-} ions were generated through a simple disproportionation reaction of element sulfur to avoid the interfering of other compounds. Fortunately, through many detailed exploring experiments, several S_2^{2-} doped TiO_2 nanotubes with different S_2^{2-} contents (0.26 At%–0.33 At%) have been prepared under 500° C for 2 h. The products exhibit a full visible-light absorption (from 400 to 800 nm) and a greatly enhanced photocatalytic H_2-production rate under visible-light irradiation (9610 $\mu mol\, h^{-1}\, g^{-1}$, about 13.7 and 37 times of other cationic and anion S-doped TiO_2 nanoparticles, respectively, almost highest in all the results reported previously in literatures of TiO_2 doped with non-metal elements, as shown in Table 1).

2. Experimental section

2.1. Synthesis of anionic S_2^{2-}-doped TiO_2 nanotubes

All of the chemicals were of analytical grade and were used as received. TiO_2 nanotube precursors were synthesized according to the literature [28]. The sublimed sulfur powders and TiO_2 nanotubes were equably mixed in a combustion boat. The mixture then was transferred to tube furnace and heated to 500 °C at the speed of 10 °C min^{-1} for 2 h in Ar atmosphere to avoid the simple oxidation. The obtained simples soaked in a solution of dimethylbenzene for 10 h, to remove sulfur particles, and then rinsed with ethanol and deionized water several times. In order to remove the surface-adsorbed SO_4^{2-} or SO_3^{2-} species, the samples were treated with a solution of 0.1 M HCl for 10 h, and then rinsed with deionized water many times. The washed samples were dried at 80 °C for 24 h and S-doped TiO_2 nanotubes were produced.

2.2. Characterization

All the samples in following each measurement were added in the same amount. Final products were examined by X-ray powder diffraction (XRD) analysis was carried out with a Japan Rigaku

D/max-rA X-ray diffractometer with graphite monochromatized Cu-Ka radiation (α = 1.54178 Å) and an accumulative detector. The scan rate of 0.05° s^{-1} was used to record the patterns in the 2 h range of 20°–70°. Scanning electron microscopy (SEM) images were taken with a JEOL-5600LV scanning electron microscope, using an accelerating voltage of 20 kV. Transmission electron microscopy (TEM) and the high-resolution transmission electron microscopic (HRTEM) images of S-doped TiO_2 nanotubes were obtained with a JEOL HRTEM (JEM2010 electron microscope) with an accelerating voltage of 200 kV. The Brunauer Emmett Teller (BET) specific surface area (SBET) of the powders was analyzed by nitrogen adsorption in a Micromeritics ASAP 2020 nitrogen adsorption apparatus (U.S.). All of the prepared samples were degassed at 60 °C prior to nitrogen adsorption measurement nanotubes. The BET surface area was determined by a multipoint BET method using the adsorption data in the relative pressure (P/P°) range of 0.05-0.3. The desorption isotherm was used to determine the pore size distribution using the Barret-Joyner-Halender (BJH) method, assuming a cylindrical pore modal. X-ray photoelectron spectroscopy (XPS) data were obtained by an ESCALab220i-XL electron spectrometer from VG Scientific using 300W Al KR radiation. The base pressure was about 3×10^{-9} mbar. The binding energies were referenced to the C 1 s line at 285.0 eV from adventitious carbon. The room-temperature photoluminescence (PL) spectra were collected by a spectrophotometer of Jobin Yvon Fluorolog 3-221 using a Xe lamp (450 W) as excitation source. The photocurrent measurements were recorded on a semiconductor characterization system (Keithley 4200 SCS) with a Lakeshore probe station and a xenon lamp (300 W, λ > 400 nm). The electrical conductivity of samples at room temperature was obtained by a standard four-probe method using a Keithley 196 System DMM digital multimeter and an Advantest R1642 programmable dc voltage/current generator as the current source. UV–vis diffused reflectance spectra of the samples were obtained from a UV–vis spectrophotometer (UV2550, Shimadzu, Japan). $BaSO_4$ was used as a reflectance standard. The calculation method of band gap is according to the Kubelka-Munk equation:
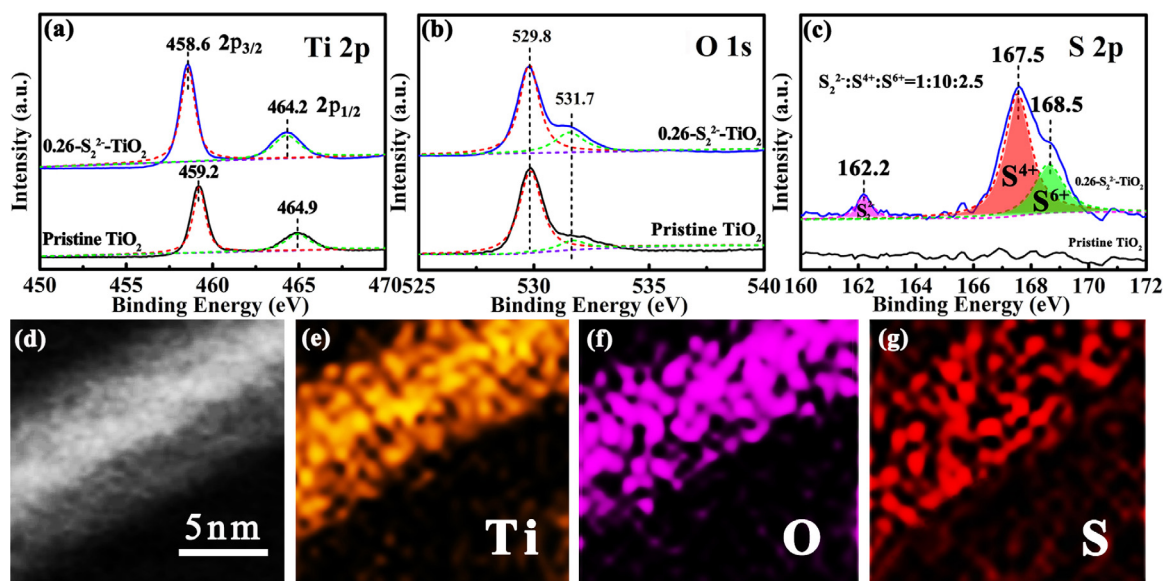
$$F(R) = \frac{(1 - R)^2}{2R}$$

where R is the percentage of reflected light. The incident photon energy (hν) and the optical band gap energy (Eg) are related to the transformed Kubelka-Munk function, $[F(R)h\nu]^p = A(h\nu - Eg)$, where Eg is the band gap energy, A is the constant depending on transition probability and p is the power index that is related to the optical absorption process. Theoretically p equals to 1/2 or 2 for an indirect or a direct allowed transition.

2.3. Photocatalytic hydrogen production

The photocatalytic hydrogen production experiment nanotubes were performed in a 500 mL quartz flat-bottom container, the openings of which were sealed with a silicone rubber septum, at ambient temperature and atmospheric pressure. A 300 W xenon arc lamp was used as a visible light source to trigger the photocatalytic reaction and was positioned at the behind of the reactor. The focused intensity on the flask was ca. 180 mW cm^{-2} to make

Table 1
Comparison of photocatalytic activity in hydrogen production from water splitting over TiO_2-based photocatalyst.

Photocatalyst	Incident light	Cocatalyst	H_2 evolution rate ($\mu mol\, h^{-1}\, g^{-1}$)	Reference
Vacuum activated TiO_2 nanoparticles	λ > 400 nm	Pt	120	Chem. Commun. [24]
Sub–10 nm TiO_2 nanoparticles	λ > 400 nm	Pt	1954	Nat. Commun. [25]
S^{4+}/S^{6+}-doped TiO_2 nanocrystals	λ > 400 nm	–	700	Catal. Commun. [20]
S^{2-}-doped TiO_2 nanocrystals	λ > 400 nm	Pt	258	J. Am. Chem. Soc. [26]
S_2^{2-}-doped TiO_2 nanotubes	λ > 400 nm	Pt	9610	This Work

Fig. 1. (a), (b) and (c) XPS spectra of Ti 2p, O 1s, S 2p peaks of the pristine TiO_2 nanotube and 0.26-S_2^{2-}-TiO_2 nanotube, respectively. (d), (e), (f) and (g) TEM image of 0.26-S_2^{2-}-TiO_2 nanotube and its corresponding EDS element mapping of Ti, O and S.

sure that the actual intensity of the liquid surface should been reached to 100 mW cm^{-2}, which was measured by an FZ-A visible-light radiometer (made in the photoelectric instrument factory of AuLight, Beijing, China) over the wavelength in the range of 400–780 nm. The photocatalytic hydrogen evolution from water was conducted using an online photocatalytic hydrogen production system (AuLight, Beijing, CEL-SPH2N). The 0.1 g of as-obtained samples were places in a mixture of 100 mL of mixed aqueous solution containing 80 mL water and 20 mL methanol in a quartz reactor. The focused intensity on the flask was measured by a visible light radiometer (made in the photoelectric instrument factory of Beijing Normal University, China). Prior to the reaction, the mixture was stirred to remove O_2 and CO_2 dissolved in water. Gas evolution was observed only under photo-irradiation and analyzed using an online gas chromatograph (SP7800, TCD, molecular sieve 0.5 nm, N_2 carrier, Beijing Keruida Limited).

The apparent quantum efficiency (QE) was measured under the same photocatalytic reaction condition, which choose the 420 nm optical filter (made in the photoelectric instrument factory of AuLight, Beijing, China) to install xenon arc lamp as light sources to
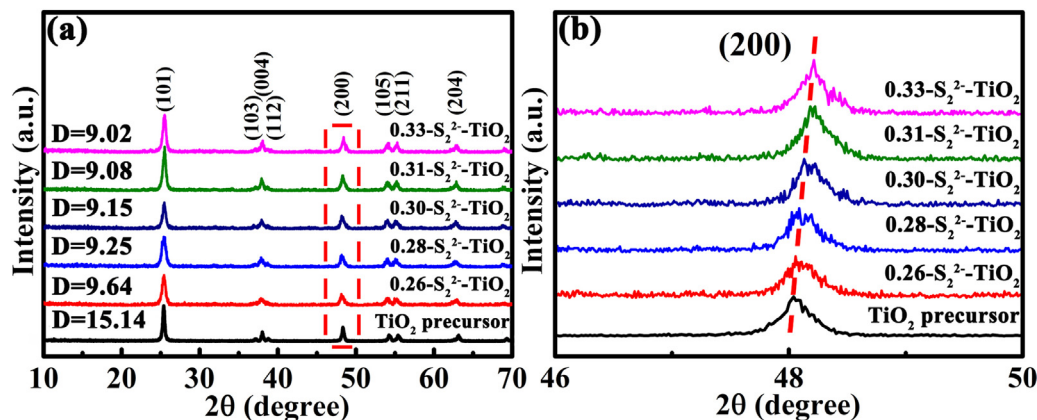
trigger the photocatalytic reaction. The QE was calculated according to equation:

$$QE [\%] = \frac{\text{number of reacted electrons}}{\text{number of incident photons}} \times 100\%$$

$$= \frac{\text{number of evolved } H_2 \text{ molecules} \times 2}{\text{number of incident photons}} \times 100\%$$
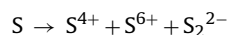
3. Results and discussion

The chemical composition measurements with X-ray photoelectron spectroscopy (XPS) of the above as-obtained products were carried out firstly, as shown in Fig. 1a–c, Fig. S1 and S2 . As expected, similar peaks due to species containing Ti, O and S in all products are presented in the wide scan XPS spectra. In 0.26-S_2^{2-}-TiO_2 sample's Ti 2p spectra (Fig. 1a), two peaks at binding energies of 458.6 and 464.2 eV, assignable to its $2p_{3/2}$ and $2p_{1/2}$, respectively, of Ti^{4+} in TiO_2 [29], are observed for all the S_2^{2-}-doped TiO_2 samples, which slightly shift to lower binding energies to compare with pure TiO_2

Fig. 2. (a) XRD patterns of sample TiO_2 nanotube precursor and S_2^{2-}-doped TiO_2 with different atomic percentage. (b) The diffraction peaks of S_2^{2-}-doped TiO_2 (200) planes with different atomic percentage.

and S^{4+}/S^{6+} doped TiO_2 in literature [22,30]. It is mainly due to the effect of as-doped S_2^{2-} ions. In O 1 s spectra (Fig. 1b), both pristine TiO_2 nanotube and 0.26-S_2^{2-}-TiO_2 nanotube have a well formed peak at 529.6 eV and a shoulder peak at 531.7 eV, which are attributed to the lattice oxygen in TiO_2 [31] and physisorbed water [32], respectively. In S 2p spectra (Fig. 1c), it is apparent that the S 2p peaks around 162.2 eV, 167.5 eV and 168.5 eV are in conformity with the reported binding energies of sulfur in S_2^{2-}, S^{4+} and S^{6+} [33–37]. In most cases, the replacement of Ti^{4+} by S^{4+}/S^{6+} in this sulfidizing process is chemically more favorable than that of O^{2-} by S^{2-} or S_2^{2-} [38]. According to previous theoretical calculation, cationic configurations (S^{4+} and S^{6+}) can be strongly stabilized in a wide range of oxygen chemical potential [23]. According to our literatures, there is no report about the observation of S_2^{2-} doped TiO_2 in experiment. It is obvious that the generation of S_2^{2-} is attributed to the disproportionation reaction of S atom itself as follows:

$$S \rightarrow S^{4+} + S^{6+} + S_2^{2-}$$

According to the XPS analysis, the contents of sulfur in TiO_2 matrixes obtained by us are 3.55, 3.81, 4.04, 4.09 and 4.39 At%, respectively. To further research the ratio of three kinds of sulfur ions, the three kind peak areas have been calculated and in the above samples their S_2^{2-}: S^{4+}: S^{6+} are 1:10:2.5, 1:9.3:3.3, 1:9.1:3.4, 1:9.2:3.1 and 1:9:3.4, respectively, as shown in Fig. 1c and Fig. S2. Correspondingly, their S_2^{2-} molar contents are 0.26 At%, 0.28 At%, 0.30 At%, 0.31 At% and 0.33 At%, respectively. The above content values are close, which means that in the present experimental conditions the S_2^{2-} content is difficult to be increased greatly because cationic S-doping of TiO_2 (S^{4+} or S^{6+}) is much more stable than anionic doping [39,40].

In addition to the XPS investigations, energy-dispersive X-ray spectroscopy (EDS) mapping is carried out to verify the three elements' distribution. Using 0.26-S_2^{2-}-TiO_2 product as an example, as shown in Fig. 1d–g, it clearly shows the presence of Ti, O and S elements and the S ions are uniformly distributed in the nanotubes, which agrees with the XPS analysis. Note that the as-prepared S_2^{2-}-doped TiO_2 samples have been washed with 0.1 M HCl solution and deionized water for many times to remove the possible surface-adsorbed SO_4^{2-} or SO_3^{2-} etc. species.

After that, XRD patterns were recorded for the dried TiO_2 powder with different S_2^{2-}-doped percentage. Fig. 2a shows their XRD patterns and pure anatase TiO_2 reported in literature (JCPDS 71-1166). The main diffraction peaks are indexed as the (101), (004), (200), (105), (211), (204) and (116) reflections of tetragonal TiO_2 (anatase phase). No peak for sulfur or sulfide is observed, which indicates that sulfur should have been well-dispersed in TiO_2 matrix, which agrees with its XPS and EDS mapping results. The samples' average crystallite size are calculated from the FWHM (full width at half maximum) of their (101) reflection planes (Fig. 2a) using Scherrer's formula,

$$D = \frac{k\lambda}{\beta \cos\theta}$$

where D is the crystallite size, k is a constant 0.9, λ is the wavelength of the X-ray diffraction, β is the FWHM and θ is the diffraction angle value. It is found that the as-synthesized samples have small crystallite size with an average size of around 15 nm and around 9 nm for pure TiO_2 and S_2^{2-}-doped TiO_2 respectively, as shown in Fig. S3 and Fig. 3d. From this point, it can be noticed that the addition of sulfur decreases the crystallite size of the TiO_2 nanotube precursor to some extent. Accordingly, the sulfur doping triggers a broadening effect on the XRD peaks of TiO_2. Except that, representatively, (200) reflection planes of the S_2^{2-}-doped TiO_2 samples shift to higher diffraction angles relative to pure TiO_2 (Fig. 2b), implying the lattice's shrinkage with the addition of sulfur. Considering their different ionic sizes (Ti^{4+} = 0.68 Å, S^{4+} = 0.37 Å, S^{6+} = 0.29 Å, O^{2-} = 1.4 Å and S_2^{2-} = 2.055 Å), it is comprehensible that for the content of S_2^{2-} is much less than that of S^{4+} and S^{6+}, as indicated in XPS results, the change of TiO_2 lattice size is determined mainly by the additional S^{4+} and S^{6+}, which replace the Ti^{4+} with smaller sizes.

The morphologies and microstructures of S_2^{2-}-doped TiO_2 nanotubes are characterized by SEM, TEM and HRTEM examinations, as shown in Fig. 3 and Fig. S4. As shown in the SEM images of 0.26-S_2^{2-}-doped TiO_2 nanotubes (Fig. 3a and b), the 1D nanostructures have extraordinarily smooth surfaces, and are up to 2 μm in

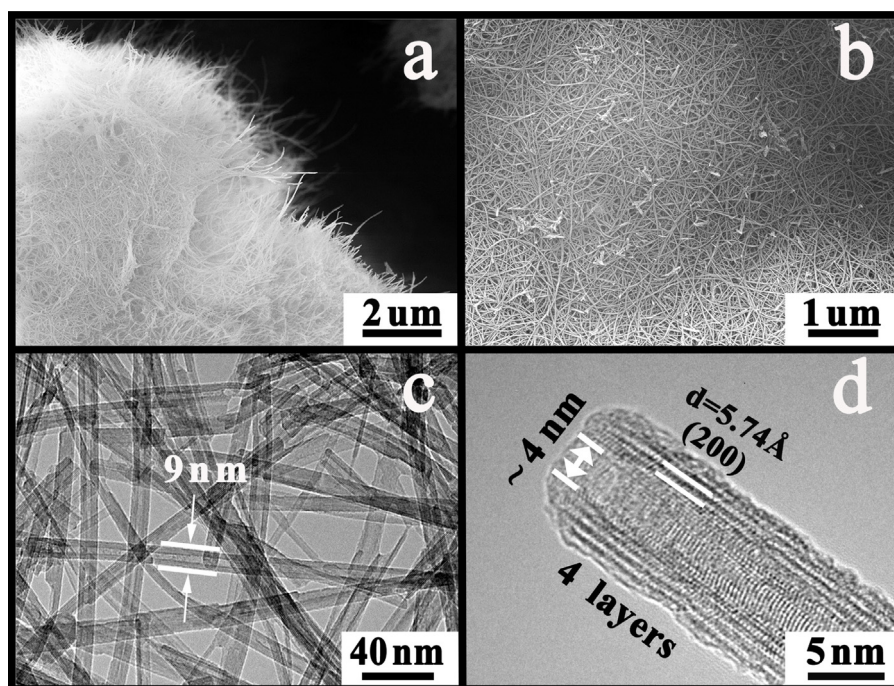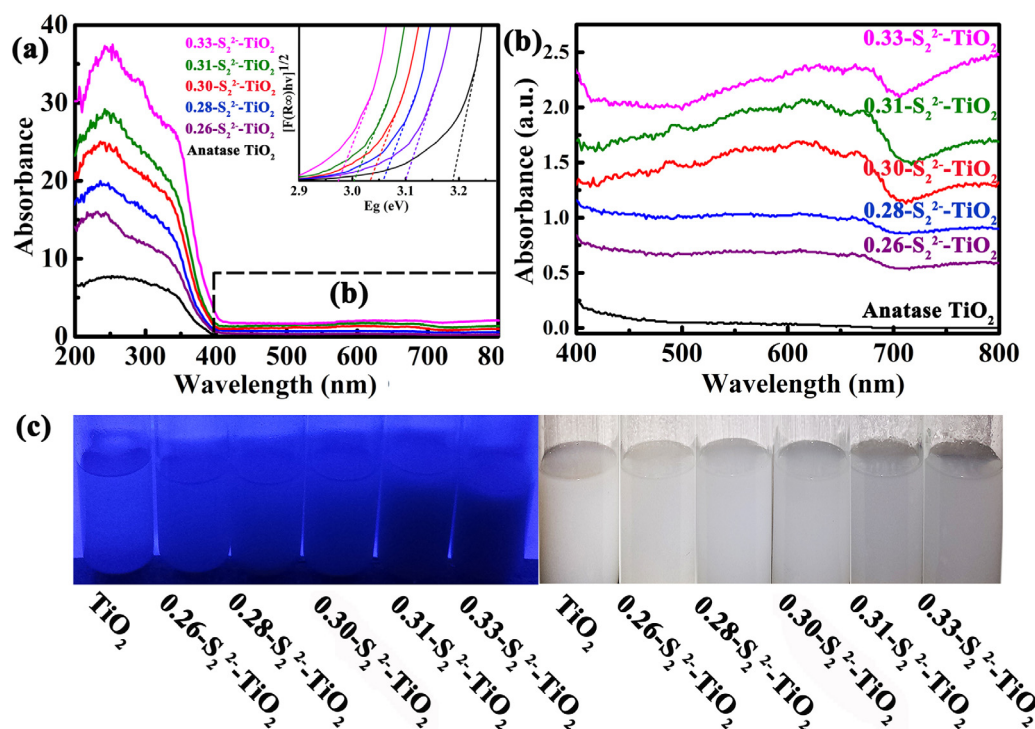**Fig. 3.** (a) and (b) SEM images of simple 0.26-S_2^{2-}-doped TiO_2 nanotubes, (c) TEM image and (d) HRTEM image of simple 0.26-S_2^{2-}-doped TiO_2 nanotubes.

Fig. 4. (a) UV–visible diffuse reflectance spectra of the undoped TiO_2 and S_2^{2-}-doped TiO_2 samples, respectively; the inset shows the plots of $[F(R_\infty)h\nu]^{1/2}$ versus $h\nu$ for band gap energies. (b) The enlarged graph of (a) in the range of 400–800 nm. (c) A photograph of the TiO_2 nanotubes and S_2^{2-}-doped TiO_2 nanotubes under ultraviolet light and visible light, respectively.
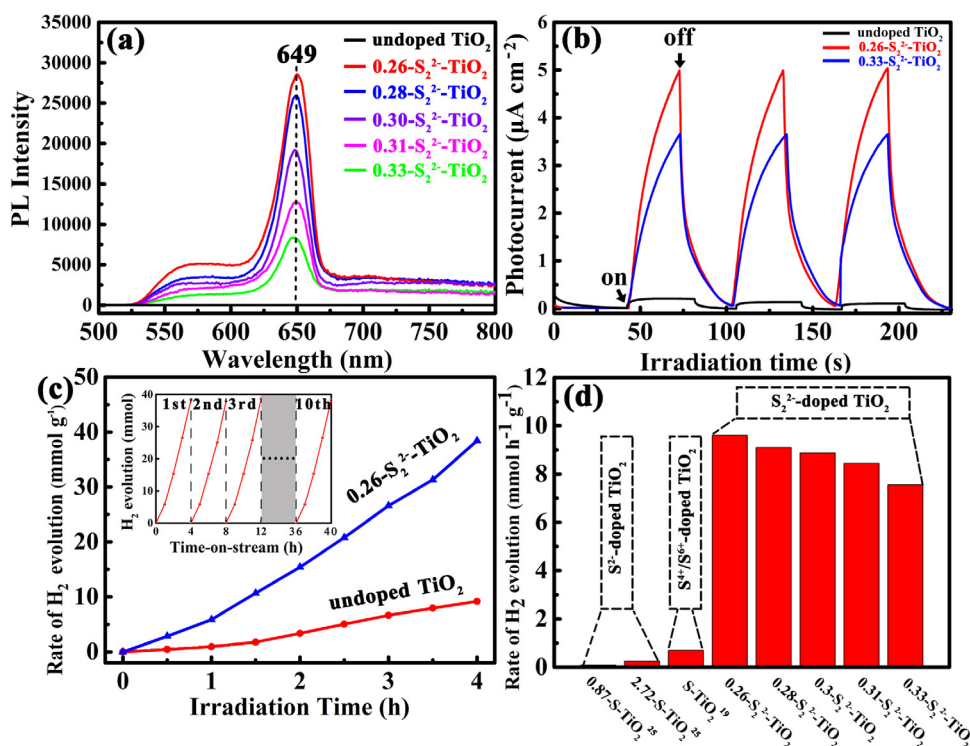
length. It is clear that the S_2^{2-}-doped TiO_2 nanotubes have a highly oriented growth behavior and fairly high aspect ratio (∼200, i.e. length divided by diameter), which may improve their physico-chemical activities. Their corresponding typical TEM and HRTEM images are shown in Fig. 3c and d. The nanotube's diameter is 9 nm, and the tube-wall is about 2.5 nm and composed of 4 layers nanotube walls and the interlayer spacing is about 5.74 Å, which is consistent with the treble lattice distance of (200) plans. It is comprehensible that the nanotubes rolled with the atom layers will more effectively favor the S_2^{2-} ions' diffusion and doping process and also inhibit the recombination of the electron-hole pairs in them compared with the block structures [24,41,42].

The favorable specific surface area is expected to accommodate a large amount of superficially active sites to participate in photo-catalysis hydrogen evolution reactions. So the porosity and surface area of the TiO_2 nanotube precursor and $S-TiO_2$ nanotubes are examined firstly by N_2 adsorption- desorption measurements. As showed in Fig. S5, typical Langmuir type IV characteristic isotherms accompanied by hysteresis loops are observed in all the samples, suggesting the formation of a porous structure. It can be seen in Table S1 that compared with the TiO_2 nanotube precursor, the BET surface areas of the S_2^{2-}-doped TiO_2 samples show an increase from 54.5 $m^2\,g^{-1}$ to 118.1 $m^2\,g^{-1}$, which is due to the smaller crystallite sizes, as showed in Table S1. The relatively high specific area could facilitate the diffusion of reactant molecules and offer more active sites for adsorption, resulting in a more efficient photocatalytic process. It is noticed in the inset of Fig. S5 that TiO_2 nanotubes have a pore size at around 5.5 nm. When sulfur is introduced, mesoporous begin to shrink to a pore size at around 3.5 nm. All the above results confirm the similarity on the morphologies and structures of the as-obtained $S-TiO_2$ products.

It has been predicted though a theory calculation that anionic S_2^{2-} showed completely different spectral behaviors compared with that of undoped TiO_2 and TiO_2 doped of cationic S^{4+} and S^{6+},

which had never been observed in the experimental optical spectra for S_2^{2-}-doped TiO_2. Anionic S_2^{2-} doped TiO_2 possessed a very wide UV and visible-light absorption region [23]. Correspondingly, a series of S_2^{2-}-doped TiO_2 nanotubes have been dispersed in the solvent of ethanol. Fig. 4c displays the sample pictures of suspensions of $S-TiO_2$ nanotubes with a same concentration under visible light and ultraviolet light respectively. Clearly, with the increasing of sulfur-doping content, the color of the products change from milky-white to grayer under visible light and from lucency to dark under ultraviolet light (365 nm), which indicates their absorption spectra ranging from UV region to visible-light region. Meanwhile, their UV–vis diffuse reflectance spectra further confirm the above observation, as shown in Fig. 4a and b. There is an enhanced absorbance in the UV region and visible-light region (>400 nm) with increasing sulfur content. The plots of transformed K-M function versus the energy of light (the inset of Fig. 4a) give band-gap energies of pristine TiO_2 and S_2^{2-}-doped TiO_2 with the different contents, respectively. In addition, the shapes of the spectra are similar to the UV–vis one predicted in theory calculation [23]. Many experimental results proved a red-shift (near 400 nm) in the optical absorption edge of cationic S^{4+} and/or S^{6+} doped TiO_2 with respect to that of undoped TiO_2 [43,44]. However, the full visible-light absorption of S_2^{2-}-doped TiO_2 has never been reported according to our literatures. According to the DOS calculations, it has been confirmed that anionic S_2^{2-} doping in TiO_2 will provide new occupied and strongly localized electronic states in the gap, located at 0.9–1.6 eV above the valence band of TiO_2, which results in the broad visible-light absorption [23].

In order to investigate their practical production rate of free electrons after a visible-light absorption, comparable PL measurements with a same addition amount using a 500 nm visible-light excitation wavelength have been conducted, as shown in Fig. 5a. It can be seen that the PL emission signals of S_2^{2-}-doped samples are observed from 525 to 800 nm in the visible region and

Fig. 5. (a) Visible-light driven photocatalytic water splitting for H$_2$ generation by undoped TiO$_2$ nanotube and 0.26-S$_2^{2-}$-TiO$_2$ nanotube. Inset pattern is the cycling stability results of photocatalytic H$_2$ production over 0.26-S$_2^{2-}$-TiO$_2$. (b) The comparison of the photocatalytic H$_2$ production activities of the S$_2^{2-}$-TiO$_2$ with different sulfur doping mounts.

centered at 649 nm (1.91 eV). In contrast, no PL emission signal of undoped TiO$_2$ has been detected, which agrees with its non-absorption in the above UV–vis result (Fig. 4b). Besides, it is also found that with the increase of S doping content, their PL emission intensities decrease, indicating less free electrons produced after a visible-light absorption. Furthermore, the generation and transport efficiency of the excited electron for S$_2^{2-}$-doped and undoped TiO$_2$ nanotubes are also studied by comparable transient photocurrent response experiments under visible-light irradiation, as shown in Fig. 5b. When the light is successively switched on and off, a series of signals are obtained for undoped TiO$_2$, 0.26-S$_2^{2-}$-TiO$_2$ and 0.33-S$_2^{2-}$-TiO$_2$. Consistent with their PL results, it shows that the 0.26-S$_2^{2-}$-TiO$_2$ sample has the most enhanced photocurrents under visible light. In fact, it has been pointed out in our XPS results that the anionic S$_2^{2-}$ doping contents in all treated TiO$_2$, which preside over the visible-light absorption, are very close. So the main difference in the doped sulfur focuses on the cationic S^{4+} and S^{6+} contents. Afterward, the conductivities of undoped TiO$_2$, 0.26-S$_2^{2-}$-TiO$_2$ and 0.33-S$_2^{2-}$-TiO$_2$ have also been measured, which are 1.3×10^9, 3.16×10^7 and 2.21×10^8 Ω, respectively. So the decrease of the visible-light generated free electron amounts are due to the weakened conductivities with the increase of sulfur doping quantities.

Recently, Yang et al. synthesized 0.87 At% and 2.72 At% S^{2-} doped TiO$_2$ nanoparticle, which displayed max H$_2$-production rates of 30 μmol h^{-1} g^{-1} and 258 μmol h^{-1} g^{-1}, respectively [26]. Zhang et al. synthesized S^{4+}/S^{6+} doped TiO$_2$ nanoparticle, which displayed max H$_2$-production rates of 700 μmol h^{-1} g^{-1} [20]. In this our work, under visible light (400 nm < λ < 800 nm, Fig. 5c), 0.26-S$_2^{2-}$-TiO$_2$ nanotubes exhibit the highest mass-specific activity (9610 μmol h^{-1} g^{-1}) and the quantum efficiency is 19.8% at 420 nm, as shown in Table S1, consistent with their absorbance ability to visible light. The H$_2$-production rate of our sample is 13.7 and 37 times of that cationic and anion S-doped TiO$_2$ obtained in the above litera-

ture, as shown in Fig. 5d. In addition, our H$_2$-production rate is much higher than all S-doped materials reported in literatures, as shown in Table 1. More importantly, though S$_2^{2-}$ doped TiO$_2$ is deemed metastable [23], S$_2^{2-}$-TiO$_2$ nanotubes prepared by us exhibit very good stability as photocatalysts. We have conducted XPS measurements of the pristine TiO$_2$ nanotube and 0.26-S$_2^{2-}$-doped TiO$_2$ nanotube after the photocatalytic experiments, as shown in Fig. S6. From Fig. S6a and b, we can see that the main peaks of both Ti 2p and O 1s are unchanged after tests. Moreover, the peak of S$_2^{2-}$ still exists in the spectrum (Fig. S6c). However, after tests, both pristine TiO$_2$ nanotube and 0.26-S$_2^{2-}$-doped TiO$_2$ nanotube are observed shoulder peaks at 531.2 eV, which are attributed to the hydroxyls [45]. It has been proved that, during the photocatalytic tests, the surfaces of nanotubes have been irradiated and generated both electrons and holes. The electrons are combined with H$^+$ to form H$_2$ and the holes are combined with OH$^-$ to form −OH [46,47]. We also provide the cycling stability tests in Fig. 5c (inset) and no noticeable decrease in the activity for photocatalytic hydrogen production is observed, which further proves the S$_2^{2-}$ stability in TiO$_2$ nanotubes. Therefore, the remarkable activity and stability make S$_2^{2-}$-TiO$_2$ nanotube a promising semiconductor photocatalyst candidate for hydrogen production from water splitting under visible light. Consistent with the PL and photocurrent response test results, it is also found that a further increase of sulfur content leads to a deterioration of the catalytic performance, as shown in Fig. 5a and b. As a consequence, a suitable content of sulfur is crucial for optimizing the photocatalytic activity of S$_2^{2-}$-doped TiO$_2$ nanotubes. Most importantly, the doping of anionic S$_2^{2-}$ is the critical factor for the enhanced photocatalytic H$_2$-production.

4. Conclusions

In summary, through a simple disproportionation reaction of element sulfur, anionic S$_2^{2-}$ has been successfully doped into TiO$_2$

nanotubes with different sulfur contents, which induced a full visible-light absorption S and an enhanced visible-light photogenerated electron rate. Correspondingly, the as-obtained S_2^{2-}-TiO_2 samples exhibit high efficiencies (up to 9610 μmol h^{-1} g^{-1}) and an apparent quantum efficiency (19.8% at 420 nm) of photocatalytic H_2 production from water splitting under visible-light irradiation. This work enlightens a way to the realization of a full visible-light absorption by semiconductor material through controlling the doped ionic state.

Author contributions

The manuscript was written through contributions of all authors. All authors have given approval to the final version of the manuscript.

Acknowledgments

Appendix A. Supplementary data

Supplementary data associated with this article can be found, in the online version, at http://dx.doi.org/10.1016/j.apcatb.2017.01.027.

References

[1] R.D. Cortright, R.R. Davda, J.A. Dumesic, Nature 418 (2002) 964–967.
[2] A. Fujishima, K. Honda, Nature 238 (2008) 37–38.
[3] M.R. Hoffmann, S.T. Martin, W. Choi, D.W. Bahnemann, Chem. Rev. 95 (1995) 69–96.
[4] L. Thompson, J. Yates, Chem. Rev. 106 (2006) 4428–4453.
[5] D. Ravelli, D. Dondi, M. Fagnoni, A. Albini, Chem. Soc. Rev. 39 (2009) 1999–2011.
[6] M. Hernández-Alonso, F. Fresno, S. Suárez, J. Coronado, Energy Environ. Sci. 2 (2009) 1231–1257.
[7] S.J. Moniz, S.A. Shevlin, D.J. Martin, Z. Guo, J. Tang, Energy Environ. Sci. 8 (2015) 731–759.
[8] X. Chen, S. Mao, Chem. Rev. 107 (2007) 2891–2959.
[9] R. Asahi, T. Morikawa, T. Ohwaki, K. Aokiv, Y. Taga, Science 293 (2001) 269–271.
[10] S.U. Khan, M. Al-Shahry, W. Ingler Jr., Science 297 (2002) 2243–2245.
[11] S. Sakthivel, H. Kisch, Angew. Chem. Int. Ed. 42 (2003) 4908–4911.
[12] J.H. Park, S. Kim, A.J. Bard, Nano Lett. 6 (2006) 24–28.
[13] S. Hoang, S. Guo, N. Hahn, A.J. Bard, C.B. Mullins, Nano Lett. 12 (2002) 26–32.
[14] W. Zhao, W. Ma, C. Chen, J. Zhao, Z. Shuai, J. Am. Chem. Soc. 126 (2004) 4782–4783.
[15] T. Umebayashi, T. Yamaki, H. Itoh, K. Asai, Appl. Phys. Lett. 81 (2002) 454–456.
[16] X. Chen, C. Burda, J. Am. Chem. Soc. 130 (2008) 5018–5019.
[17] S.Y. Arman, H. Omidvar, S.H. Tabaian, M. Sajjadnejad, Sh. Fouladvand, Sh. Afshar, Surf. Coat. Technol. 251 (2014) 162–169.
[18] L. Jia, C. Wu, Y. Li, S. Han, Z. Li, B. Chi, J. Pu, L. Jian, Appl. Phys. Lett. 98 (2011) 211903.
[19] M. Zhu, C. Zhai, L. Qun, C. Lu, A.S. Paton, Y. Du, M.C. Goh, ACS Sustain. Chem. Eng. 3 (2015) 3123–3129.
[20] W. Zhang, S. Wang, J. Li, X. Yang, Catal. Commun. 59 (2015) 189–194.
[21] S.M. El-Sheikh, G. Zhang, H.M. El-Hosainya, A.A. Ismail, K.E. O'shea, P. Falarasd, A.G. Kontos, D.D. Dionysiou, J. Hazard. Mater. 280 (2014) 723–733.
[22] Y. Lin, S. Chou, H. Chu, J. Nanopart. Res. 16 (2014) 2539.
[23] M. Harb, P. Sautet, P. Raybaud, J. Phys. Chem. C 117 (2013) 8892–8902.
[24] M. Xing, J. Zhang, F. Chen, B. Tian, Chem. Commun. 47 (2011) 4947–4949.
[25] L. Li, J. Yan, T. Wang, Z. Zhao, J. Zhang, J. Gong, N. Guan, Nat. Commun. 6 (2014) 5881–5891.
[26] C. Yang, Z. Wang, T. Lin, H. Yin, X. Lu, D. Wan, T. Xu, C. Zheng, J. Lin, F. Huang, X. Xi, M. Jiang, J. Am. Chem. Soc. 135 (2013) 17831–17838.
[27] T. Ohno, T. Umebayashi, K. Asai, T. Mitsui, M. Matsumura, Appl. Catal. A 265 (2004) 115–121.
[28] W. Liu, P. Gao, D. Bao, G. Zhang, Y. Chen, G. Chen, Y. Wang, L. Wang, S. Yang, G. Li, Y. Sun, RSC Adv. 3 (2013) 6531–6537.
[29] D. Scanlon, C. Dunnill, J. Buckeridge, S.A. Shevlin, A. Logsdail, S. Woodley, C.R. Catlow, M.J. Powell, R. Palgrave, I. Parkin, G. Watson, T. Keal, P. Sherwood, A. Walsh, A. Sokol, Nat. Mater. 12 (2013) 798–801.
[30] J. Ni, S. Fu, C. Wu, J. Maier, Y. Yu, L. Li, Adv. Mater. 28 (2016) 2259–2265.
[31] A. Naldoni, M. Allieta, S. Santangelo, M. Marelli, F. Fabbri, S. Cappelli, C.L. Bianchi, R. Psaro, V. Dal Santo, J. Am. Chem. Soc. 134 (2012) 7600–7603.
[32] G. Ketteler, S. Yamamoto, H. Bluhm, K. Andersson, D.E. Starr, D.F. Ogletree, H. Ogasawara, A. Nilsson, M. Salmeron, J. Phys. Chem. C 111 (2007) 8278–8282.
[33] T. Matsuyama, M. Deguchi, K. Mitsuhara, T. Ohta, T. Mori, Y. Orikasa, Y. Uchimoto, Y. Kowada, A. Hayashi, M. Tatsumisago, J. Power Sources 313 (2016) 104–111.
[34] P. Velásquez, D. Leinen, J. Pascual, J.R. Ramos-Barrado, P. Grez, H. Gómez, R. Schrebler, R.D. Río, R. Córdova, J. Phys. Chem. B 109 (2005) 4977–4988.
[35] F. Dong, W. Zhao, Z. Wu, Nanotechnology 19 (2008) 365607.
[36] J. Xu, J. Li, W. Dai, Y. Cao, H. Li, K. Fan, Appl. Catal. B: Environ. 79 (2008) 72–80.
[37] J.C. Yu, W.K. Ho, J.G. Yu, H. Yip, P.K. Wong, J.C. Zhao, Environ. Sci. Technol. 39 (2005) 1175–1179.
[38] X. Tang, D. Li, J. Phys. Chem. C 112 (2008) 5405–5409.
[39] V.K. Gudelli, V. Kanchana, S. Appalakondaiah, G. Vaitheeswaran, M.C. Valsakumar, J. Phys. Chem. C 117 (2013) 21120–21131.
[40] B. Yu, X. Zhang, Y. Jiang, J. Liu, L. Gu, J. Hu, L. Wan, J. Am. Chem. Soc. 137 (2015) 2211–2214.
[41] V.B. Dmitry, M.F. Jens, C.W. Frank, Adv. Mater. 18 (2006) 2807–2824.
[42] T. Kasuga, M. Hiramatsu, A. Hoson, T. Sekino, K. Niihara, Adv. Mater. 11 (1999) 1307–1311.
[43] T. Ohno, M. Akiyoshi, T. Umebayashi, K. Asai, T. Mitsui, M. Matsumura, Appl. Catal. A 265 (2004) 115–121.
[44] Y. Wang, J. Li, P. Peng, T. Lu, L. Wang, Appl. Surf. Sci. 254 (2008) 5276–5280.
[45] Y. Wang, H. Sun, X. Duan, H.M. Ang, M.O. Tadé, S. Wang, Appl. Catal. B 172 (2015) 73–81.
[46] J. Yu, Q. Xiang, M. Zhou, Appl. Catal. B 90 (2009) 595–602.
[47] O. Bikondoa, C.L. Pang, R. Ithnin, C.A. Muryn, H. Onishi, G. Thornton, Nat. Mater. 5 (2006) 189–192.